PHYSICAL REVIEW A VOLUME 22, NUMBER 5 NOVEMBER 1980

Kinetics of nucleation in a binary liquid mixture

S. Krishnamurthy and W. I. Goldburg
Department of Physics and Astronomy, University of Pittsburgh, Pittsburgh, Pennsylvania 15260
(Received 16 June 1980)

Using a microscope, we have studied the formation and growth of nuclei in a supercooled binary liquid mixture of 2,6-lutidine and water close to the critical point. The results have been compared with a recent theoretical prediction by Langer and Schwartz. Although the observed growth is in good agreement with the diffusion model they used, their predicted nucleation rates remain untested. Our most important finding is the clear experimental evidence of the effect of critical slowing down on the phase-separation process in the nucleation regime. These observations thus account for the anomalously large supercoolings reported in liquids and binary mixtures near the critical point.

I. INTRODUCTION

Phase separation in alloys and glasses may proceed either by spinodal decomposition[1] or by nucleation.[2] In the former process the system evolves from a totally unstable initial state which is usually reached by quenching the system to well below the phase-separation temperature and into the spinodal (i.e., unstable) region of the composition-temperature phase diagram. Nucleation is associated with metastability and the existence of a thermodynamic barrier to the formation of droplets of a second phase. Pure fluids and binary mixtures are better suited than solids for the study of the kinetics of nucleation, because fluids can be highly purified and they support no internal strains or defects. Working near the critical point has the added advantages that the droplets of critical size are of macroscopic dimensions and that the nucleation takes place over conveniently measurable times.

A number of experiments on the onset of nucleation in fluids and binary mixtures near the critical point have been performed in recent years.[3-8] All these measurements in the critical region show anomalously large supercoolings, contrary to theoretical predictions.[2,9] Recent theoretical ideas[10,11] suggest that nucleation theory itself may not be at fault.

Theories of nucleation[2,9,10] ordinarily predict the rate of formation of stable embryos, i.e., droplets, of an emerging phase. This rate is a function of the degree of supercooling δT in an initially homogeneous metastable system of fixed composition. The calculated rate varies very rapidly as a function of δT, with the result that nucleation is observable only in a narrow range of this parameter. We may refer to this narrow range as the limit of metastability. This is the limit measured experimentally and found to exceed the predicted value by factors of 2 or more in the critical region. A resolution of this paradox was offered by Binder and Stauffer.[10] They argued that the experimentally meaningful quantity is not the nucleation rate itself, but the time required for the reaction to go to completion. One must then consider droplet growth as well as formation. Since the nucleation experiments have been performed in systems with locally conserved order parameter, the growth is diffusion controlled—and diffusive processes over critical length scales become very slow near the critical point.

The Binder-Stauffer program was carried out in great detail by Langer and Schwartz[11] (LS). They predicted the complete sequence of states of a phase-separating fluid starting from the quench into a supersaturated state and ending with the completion of the reaction.

In this paper we report detailed microscopic observations of nucleation and growth near the critical point in a supersaturated binary liquid mixture of 2, 6-lutidine and water (LW). In these experiments the samples were off-critical in composition. This system has an inverted coexistence curve, unlike the typical phase diagram shown in Fig. 1(a). Thus, a "quench" into the two-phase region is an upward jump in temperature from an initial state $T = T_i < T_{cx}$ to a final value T, as illustrated in Fig. 1(b). Here T_{cx} is the temperature at which the phases with compositions C_A and C_B coexist in equilibrium. The degree of supercooling (superheating here) can be expressed in terms of the quantities ΔT and δT shown in the figure. This ratio $\delta T/\Delta T$ was varied in the interval 0.1–0.5.

Phase separation was observed photographically using a 35-mm camera attached to a microscope with the magnification usually set at 50. A typical sequence of pictures is reproduced in Fig. 2. It shows droplets growing over an interval between 1 min and $1\frac{1}{2}$ h after the quench. For this run, $\Delta T = 44$ mK and $\delta T = 8$ mK. The smallest division on the scale appearing in the pictures is 20 μm. Because the droplets are not so clearly resolvable at small t, they have been inked in at the earliest

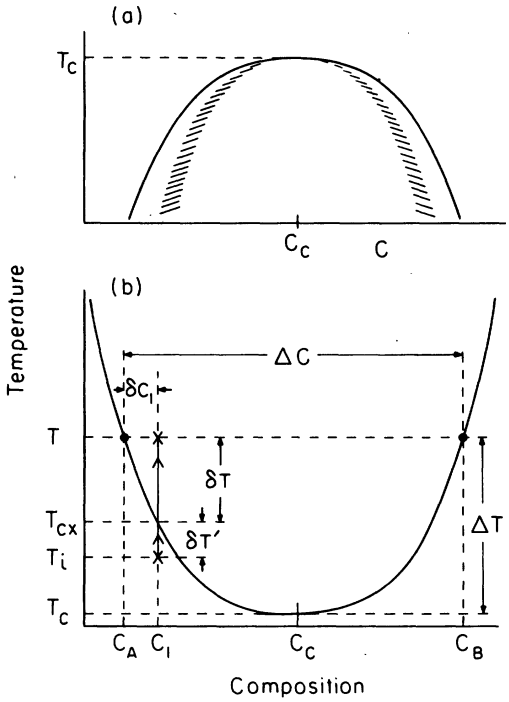

FIG. 1. The coexistence curve (solid line) and metastability limit (hatched) for a normal system (a), and the coexistence curve for one with a lower critical point (b), such as 2, 6-lutidine water. The relevant quantities defined in the text are shown in (b).

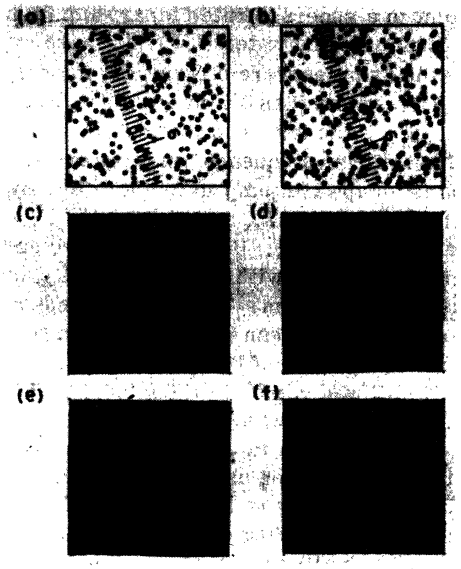

FIG. 2. Microphotographs of nucleating sample at a magnification of 50. The smallest division on the scale is 20 μm. For this run, $\Delta T = 44$ mK and $\delta T = 8$ mK. (a) and (b) are inked reproductions of the original pictures taken 58 and 127 sec after the quench. (c), (d), (e), (f), respectively, are photographs at 5.5, 13.4, 33, and 78 min after the quench.

times, viz., at 58 and 127 sec [Figs. 2(a) and 2(b), respectively]. Note that the nuclei are uniform in size at small t. The average radius of droplets in Fig. 2(b) is 4.7 ± 1 μm. Figures 2(c), 2(d), 2(e), and 2(f) are photographs at 5.5, 13.4, 33, and 78 min after the quench. These pictures provide detailed information regarding the time dependence of the droplet size distribution, the droplet density, and the supersaturation. Three samples with $\Delta T_{cx} = |T_{cx} - T_c|$ of 5, 35, and 97 mK were studied at various quench depths.

The rate of droplet formation is so strongly dependent on the supercooling that from one quench to another it was reproducible only within an order of magnitude. Thus a rigorous test of nucleation theory itself was not possible. However, the observed growth of the nuclei could be understood, using the diffusive growth model of Lifshitz and Slyozov.[12] The essential ideas of Binder and Stauffer were borne out,[10] although the most important predictions of Langer and Schwartz[11] still remain untested. Perhaps our most important finding is the clear experimental evidence of simultaneous occurrence of nucleation and growth due to critical slow down, and that the anomalous results previously reported[3-8] are unequivocally due to this effect. The remainder of the paper is divided as follows. Section II contains a brief review of the theory of Langer and Schwartz (LS).[11] Special emphasis will be given here to the scaled quantities which enter any theoretical description near the critical point. Experimental details are presented in Sec. III. The results are discussed in Sec. IV and the work is summarized in Sec. V.

II. THEORY

The problem addressed by Langer and Schwartz is that of calculating the time evolution of the system which is initially ($t = 0$) placed in a metastable supersaturated state. In Fig. 1(b) this state is represented by the coordinates (C_1, T). In classical nucleation theory,[2] the metastable phase is considered to contain "embryos" of the nucleating phase. [In the case of a binary mixture as in Fig. 1(b) these would be droplets of composition C_B but of various sizes.] An embryo may grow by accretion or it may shrink. Once an embryo exceeds a critical size, it is identified as a nucleus of the new phase, which then grows rapidly. The critical size is determined by the condition that the increase in the thermodynamic potential from the formation of the interface is equal to the decrease of the thermodynamic potential from the formation of the volume of stable phase (i.e., the nucleus). The starting point in the LS model is a Becker-Döring–type theory as developed by Zeldovich,

discussed by Frenkel,[2] and applied to the critical region by Langer and Turski.[9] This model gives the rate of formation of critical embryos (i.e., the nucleation rate) as a function of supersaturation. Langer and Schwartz coupled this "droplet birth" model with a growth model first proposed by Lifshitz and Slyozov.[12] The model considers diffusive growth of, say, a spherical droplet of radius R and uniform concentration C_B immersed in the A-phase with a small supersaturation. [See Fig. 1(b).]

Following LS, we define the parameters which enter such a formalism. In dimensionless units the supersaturation is

$$x(t)=\frac{2}{\beta}\frac{\delta C(t)}{\Delta C}\,, \tag{2.1}$$

where β is the critical exponent associated with the shape of the coexistence curve given by

$$\Delta C=[\Delta C]\epsilon^{\beta}\,. \tag{2.2}$$

The square brackets denote critical amplitudes. Similarly the reduced temperature associated with the quenched state is

$$\epsilon=\Delta T/T_c=|T-T_c|/T_c\,. \tag{2.3}$$

Note that C_A and C_B are the equilibrium values of C for two-phase coexistence at T, $\Delta C=C_B-C_A$ is the miscibility gap, and $\delta C_1=C_1-C_A$ is the initial supersaturation. The supersaturation $\delta C(t)$ decreases to zero with increasing time, and $\delta C(0)=\delta C_1$. The lever rule gives the volume fraction occupied by the B-phase droplets in terms of initial (x_1) and intermediate (x) supersaturations. The result is

$$\tfrac{1}{2}\beta[x_1-x(t)]\equiv\tfrac{4}{3}\pi\bar{R}^3(t)N(t)\,, \tag{2.4}$$

where N is the number of droplets per unit volume and $\bar{R}$ is their average radius.

A spherical droplet of radius R and uniform composition C_B, immersed in the A-phase with a small supersaturation $\delta C(t)$, will grow at the rate

$$\frac{dR}{dt}\equiv\frac{D}{R}\left(\frac{\delta C(t)}{\Delta C}-\frac{2d_0}{R}\right)\,, \tag{2.5}$$

where D is the diffusion constant and d_0 is a capillary length proportional to the surface tension σ. The capillary length is $d_0=\frac{1}{6}\xi$, where ξ is the correlation length.[11] The critical radius R^* is that for which $dR/dt=0$, whence

$$R^*=2d_0\left(\frac{\Delta C}{\delta C}\right)=\frac{4d_0}{\beta x}=\frac{2\xi}{x}\,, \tag{2.6}$$

with $\beta=\frac{1}{3}$.

Equations (2.4), (2.5), and (2.6) form the basis of the Lifshitz-Slyozov theory, which is applicable to the late stages of phase separation. The essential input in the LS model is the nucleation rate. The decay of the metastable state is governed by an activation energy, which is given in the conventional spherical droplet model as

$$\frac{\Delta E^*}{kT}=\frac{4\pi\sigma R^{*2}}{3kT}=\frac{6\pi\sigma d_0^2}{3kT\beta^2x^2}=\left(\frac{x_0}{x}\right)^2\,. \tag{2.7}$$

The temperature-independent parameter x_0 is system dependent, but should be of order unity.[8,11] The nucleation rate according to Langer and Turski is given by

$$J=P[(x/x_0),x_0,\xi,D]\exp[-(x_0/x)^2]\,, \tag{2.8}$$

with J having the units of droplets/cm^3 sec. The dependence of J on the supercooling x is mainly contained in the exponential term. In addition, LS introduce a droplet size distribution function $\nu(R)$, which contains a growth term and a birth term $j(R)$, to which we will later refer.

Assuming that only droplets of size $R>R^*$ are to be counted as part of the B phase and using a simplified approximation for the radial growth velocity, LS proceed to calculate $x(t)$, $R(t)$, and $N(t)$, where

$$N=\int_{R^*}^{\infty}\nu(R)dR\,. \tag{2.9}$$

Near the critical point these quantites are conveniently scaled in dimensionless units as follows:

$$\tau=\frac{Dx_0^3}{24\xi^2}t\,, \tag{2.10}$$

$$\rho=\frac{x_0}{2\xi}\bar{R}\,, \tag{2.11}$$

$$\rho^*=\frac{x_0}{2\xi}\bar{R}^*=\frac{x_0}{x}\equiv\frac{1}{y}\,, \tag{2.12}$$

$$y=x/x_0\,, \tag{2.13}$$

$$n=\frac{64\pi}{x_0^3}\xi^3N\,, \tag{2.14}$$

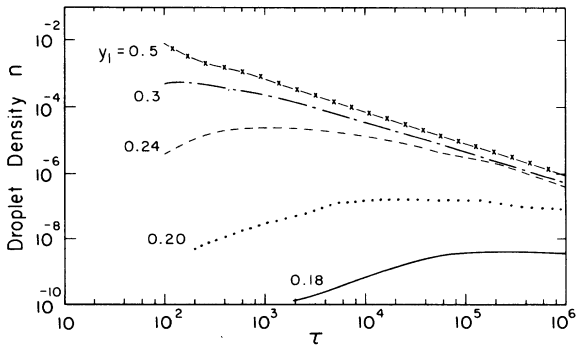

FIG. 3. Scaled density of droplets n, as a function of scaled time τ, computed by LS. The initial supersaturations y_1 are indicated for each curve.

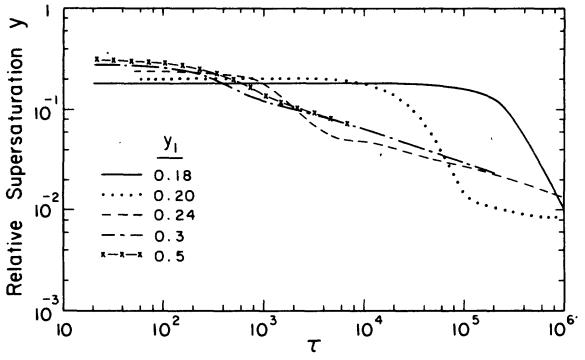

FIG. 4. Computed LS values of the relative supersaturation y as a function of τ for various initial values of y_I as indicated.

where τ is the time, ρ the mean radius, ρ^* the critical radius, y the relative supersaturation, and n the droplet density.

Figures 3, 4, and 5 show the time (τ) dependence of n, y, and ρ, respectively. These theoretical results will now be compared with our experiments carried out in the critical region.

III. EXPERIMENTAL

A. Experimental arrangement

The sample cell was located at the center of a temperature-controlled, rapidly stirred water bath. The bath temperature, which was monitored by a quartz thermometer,[13] was stable to within ±0.4 mK over 24 h and ±0.2 mK over the 2–3 h time span of a single run. The sample was illuminated by a Fiber-Lite high-intensity illuminator[14] (Series 180). Phase separation was observed with a low-power microscope[15] of a large working distance (15 cm). Over the range of magnification used (X12–X50), the depth of field was larger than 100 μm. A 35-mm camera[16] with an automatic exposure control was attached to the microscope. The photographs were taken using Kodak Plus-X Pan film with a film speed of 125 (ASA).

B. The sample cells

The LW samples were on the water-rich side of C_c. They were mixed from commercially available components[17] and sealed under atmospheric pressure. The purity of the components was 98% (2,6-lutidine) and 99.9% (water). The nominal critical parameters[18,19] for this system are $C_c = 28.70$ wt% of 2,6-lutidine and $T_c = 33.863$ °C. Figure 6 shows the design of the quartz sample cell. The reentrant cell is shown in its cross section (a) and front (b) views. The sample was illuminated from the direction shown in the figure and the microscope is focused upon the thin portion of the sample which is 0.1 mm in depth. When viewed along the line of the arrow, the cell is circular in cross section; its diameter is 2 cm. The quench was achieved by rapidly elevating the bath temperature through application of voltage pulse to a bare nichrome heater emersed in the water bath. With this heating scheme,[20] trustworthy data appeared roughly 10 sec after the bath quench.

C. Procedure

Prior to the quench, the mixture was in the one-phase region at an initial temperature T_i roughly 2 mK below the corresponding coexistence temperature. The coexistence temperature itself was first measured by cooling the mixture from the two-phase region until the droplets went back into solution (keep in mind that LW has a lower consolute point). The coarsening rate showed no dependence on $\delta T_i \equiv T_{cx} - T_i$, but it rapidly increased with quench depth $\delta T = T - T_{cx}$, where T is the final equilibrium temperature.

The photographs, generally taken at a magnifi-

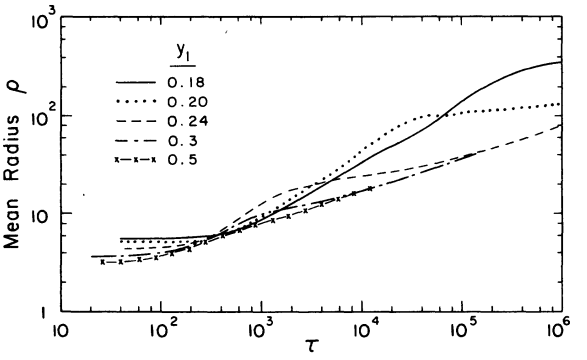

FIG. 5. Scaled mean radius ρ as a function of time τ computed by LS for various initial values of y_I as indicated.

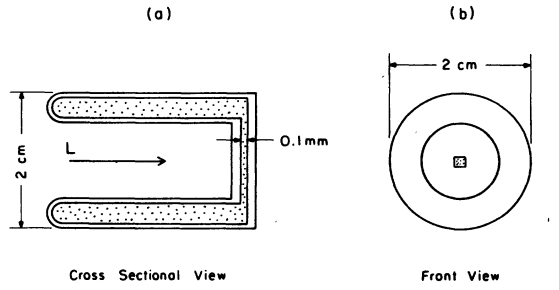

FIG. 6. Cross sectional view (a) and front view (b) of the sample cell. The cell is of reentrant type with an optical path of 0.1 mm. The direction of illumination (L) is shown. The rectangular region in (b) represents the area typically covered (1×1 mm^2) in a microphotograph.

cation of 50, exposed a portion of the sample of dimensions $1\times1\times0.1$ mm^3 as indicated in Fig. 6(b). The estimates of the droplet size were made by comparison with the scale on the reticule, which also appeared in the photographs (Fig. 2).

IV. RESULTS

The photographs were analyzed to obtain the droplet size distribution and hence the mean radius and the droplet density. It was also possible to calculate the fraction of the volume occupied by the droplets and hence estimate the leftover supersaturation, using Eq. (2.4). In this estimate, the composition inside the droplets was assumed to be that at the end of the tie line (composition C_B).

A. Droplet size distribution

Figure 7 shows the droplet size distribution at various times after the quench for the sample with $\Delta T_{cx}=35$ mK. Figures 7(a), 7(b), and 7(c) correspond to initial quench depths of $y_1=0.1$, 0.21, and 0.27, respectively. In these histograms we plot the number of droplets $N_\Omega(R)$ as a function of the radius R, in the volume (Ω) of the sample indicated on these plots.

The plots in Fig. 7(a) are for $t=301$ (——), 722 (----), 2446 (· · · ·), and 3831 (×××) sec. Here $\Omega=6.56\times10^{-5}$ cm^3. The total number of droplets in this volume, i.e., $N_{\Omega,\mathrm{tot}}(t)=\sum_R N(R)$ at the above-mentioned times is given in the caption.

Thus from Fig. 7(a) we note that the distribution is initially peaked at $R=4.7\pm0.5$ μm. The increase in the total number of droplets from 51 at 301 sec to 117 at 722 sec is due to nucleation events in this time interval. The distribution itself gets broader with time and shifts to larger sizes as the droplets grow. However the total number of droplets remains constant, within statistical

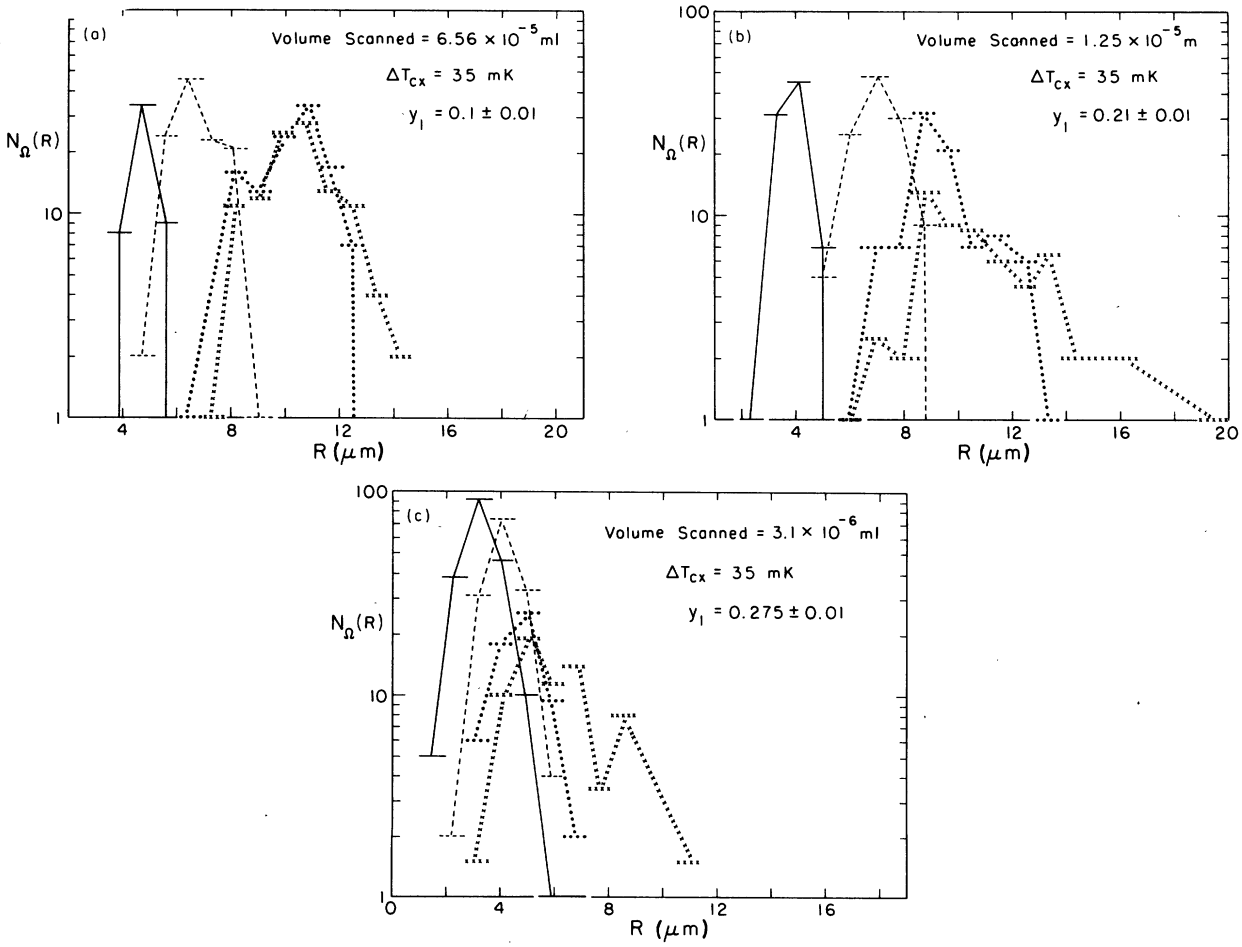

FIG. 7. Histograms showing the number of droplets $N_\Omega(R)$ as a function of the radius R in the volume (Ω) of the sample scanned at various times after the quench. The values of [t (sec), $N_{\Omega,\mathrm{tot}}(t)=\sum_R N_\Omega(R)$] are a: (301,51) ——; (722,117) ---; (2446,112) •••; and (3831,107) ×××. b: (58,84) ——; (325,117) ---; (2006,90) •••; and (4730,60) ×××. c: (58,193) ——; (450,144) ---; (1115,61) •••; and (3140,69) ×××.

TABLE I. Number of droplets $N_\Omega(R)$ of radius R in a volume $\Omega(\Delta T_{cx}=97\pm4$ mK).

	$y_1=0.11\pm0.01$ $\Omega=1.01\times10^{-4}$ cm^3				$y_1=0.20\pm0.01$ $\Omega=5.1\times10^{-5}$ cm^3					$y_1=0.27\pm0.01$ $\Omega=4.25\times10^{-6}$ cm^3			
t (sec)	179	608	961	2150		48	465	860	1435		58	227	1023
R (μm)					R (μm)					R (μm)			
2.5	1				2.5					1.8	1		
3.3	5				3.3	12				2.7	20	5	3
4.1	41				4.1	63				3.6	46	26	11
5.0	62				5.0	54				4.5	15	55	42
5.8	26				5.8	12				5.3	3	18	43
6.6	1	3			6.6	1	1			6.2		3	17
7.4		35	7	2	7.4		14	4	1	7.1			6
8.3		59	10	5	8.3		29	13	4	8.0			4
9.1		42	27	19	9.1		48	29	9				
9.9		5	47	17	9.9		53	49	16				
10.7			33	24	10.7		31	40	26				
11.6			27	27	11.6		15	34	55				
12.4			2	18	12.4		2	8	29				
13.2				12	13.2		1	1	8				
14.0				3	14.0				6				
14.9					14.9				6				
15.7				2	15.7				4				

error, after the initial increase. Further, a comparison of the plots for $t=2446$ (····) and 3831 (××××) sec, reveals the slow down of the growth process as the reaction creeps toward completion. This is due to the near-complete depletion of the supersaturation in the majority phase A.

Figure 7(b), corresponding to $y_1=0.21$, shows the distribution, initially peaked around 4 ± 1 μm at 58 sec, to broaden continuously with time. After an initial increase, attributed to nucleation events, $N_{\Omega,\mathrm{tot}}$ begins to show a drop accompanied by a broadening of the droplet size distribution with time. This is contrary to the predictions of the diffusion model used by LS [Eqs. (2.4) and (2.5)]. While the LS theory predicts a decrease in the droplet density with time (due to the dissolution of droplets that are smaller than the critical size), it should not be accompanied by a broadening of the

TABLE II. Number of droplets $N_\Omega(R)$ of radius R in a volume $\Omega(\Delta T_{cx}=5\pm0.5$ mK).

	$y_1=0.27\pm0.06$ $\Omega=9.9\times10^{-5}$ cm^3				$y_1=0.38\pm0.06$ $\Omega=4.7\times10^{-6}$ cm^3					$y_1=0.52\pm0.06$ $\Omega=2.36\times10^{-6}$ cm^3			
t (sec)	275	619	1950	2659		167	330	905	2467		135	580	1539	2636
R (μm)					R (μm)					R (μm)				
1.7	2				1.7	26	6	1		1.7	1	4		
2.6	8				2.6	67	46	20	6	2.6	33	44		1
3.4	6				3.4	15	54	78	15	3.4	50	76	3	2
4.3	12	2	1		4.3	2	9	72	34	4.3	28	25	11	7
5.2	7	17	5	1	5.2		4	15	26	5.2	4	1	21	7
6.0	2	22	6	1	6.0		1	1	33	6.0			23	9
6.9	1	31	6	1	6.9				11	6.9			5	8
7.7		26	12	1	7.7				6	7.7			1	8
8.6		5	10	4	8.6				2	8.6				1
9.5			10	7	9.5				1	9.5				3
10.3			5	6	10.3					10.3				
11.2			2	6						11.2				
12.0				9						12.0				
12.9				7						12.9				1
13.8				7										
14.6				4										
15.5				2										

distribution. It is plausible that this broadening arises from coalescence; the differential fall rate of droplets of differing sizes under gravity can cause coalescence events, even when the droplet density is not large. This limits the period of study of the growth of these droplets. Figure 7(c) is similar to Fig. 7(b), except that the effects mentioned above are more apparent because of the larger supercooling.

Tables I and II give the droplet size distribution at various initial quench depths for the samples with $\Delta T_{cx}=5$ and 97 mK. The time evolution of the reaction is qualitatively the same as for the case discussed above in detail.

B. Droplet density vs τ

Figures 8(a), 8(b), and 8(c), respectively, show n vs τ for three off-critical samples with $\Delta T_{cx}=97$, 35, and 5 mK. For each sample, the data for several quench depths are shown. The reduced units are defined in Eqs. (2.10) and (2.14). The parameter x_0 is assumed to be unity here, since none of the thermodynamic amplitudes entering the calculation of the activation energy is known for this system. For two other binary liquid mixtures,[8,11] isobutyric acid-water and perfluoromethylcyclohexane-methylcyclohexane, x_0 has been estimated to be 1.2 and 1.3, respectively.

To express our results in dimensionless units, we give the one-phase values for the diffusion constant (in cm^2/sec) and the correlation length (in cm) as quoted by Langer and Schwartz[11,19]:

$$[D]\equiv 2\times 10^{-6},$$

$$[\xi]\cong 2\times 10^{-8},$$

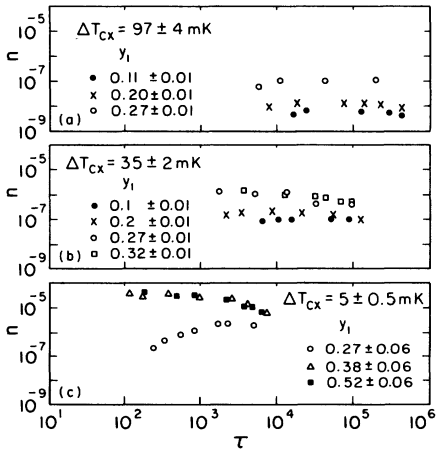

FIG. 8. Experimental values of the scaled density of droplets n as a function of time τ for three sample compositions and various initial values of y_1 as indicated.

and

$$\nu' \equiv 0.62 .$$

Consider first the measurements for the sample with $\Delta T_{cx}=35$ mK [Fig. 8(b)]. A comparison with the Langer-Schwartz theory (Fig. 3) indicates the following: The plot for $y_1=0.2$ is in fair agreement with the theoretical prediction. On the other hand, the observed droplet density is an order of magnitude smaller than predicted for $y_1=0.27$ or 0.32 but larger for $y_1=0.1$. It was not possible to reproduce the droplet density to better than an order of magnitude from one run to another with our experimental techniques. The reproducibility improved with the sample which was more off-critical ($\Delta T_{cx}=97$ mK). In this case, the observed droplet densities again exceeded the predictions for $y_1=0.11$, but were smaller for $y_1=0.2$ and $y_1=0.27$ [Fig. 8(a)].

Reproducible results were most difficult to obtain in the experiments with the sample which was the least off-critical ($\Delta T_{cx}=5$ mK). This could be attributed to the strong dependence of the nucleation rate on supercooling. For example, compare the theoretical predictions of n vs τ for $y_1=0.18$ and 0.2 in Fig. 3. From this figure one sees that an increase of only 0.02 in y_1 is expected to produce two to three orders of magnitude increase in the droplet density. Since the quench depth δT was reproducible to only within ±0.4 mK, the initial droplet density was uncontrolled near the critical point. Far from T_c, when both δT and ΔT are large, this effect is less pronounced.

Because the initial number density dictates the subsequent time evolution, further comparison between the present measurements and the numerical results of the LS theory is not meaningful. Therefore, we present an alternative analysis of our droplet growth data in the following section.

C. Mean radius vs τ; supersaturation vs τ

Figures 9(a), 9(b), and 9(c) show ρ vs τ for the three sample compositions and various initial quench depths of the previous figure. Refer to Eq. (2.11) for the definition of the dimensionless radius ρ in terms of R. The average radius was determined typically from a set of 100 to 200 droplets. Only droplets of radius larger than 3 μm could be resolved in the photographs. As a result, initial stages of nucleation could not be studied.

In Figs. 10(a), 10(b), and 10(c) we show the relative supersaturation y [defined by Eqs. (2.1) and (2.13)] as a function of τ, for the above-mentioned runs. The supersaturation is extracted from the photographs using the conservation Eq. (2.4).

The solid lines on the ρ vs τ and y vs τ plots are

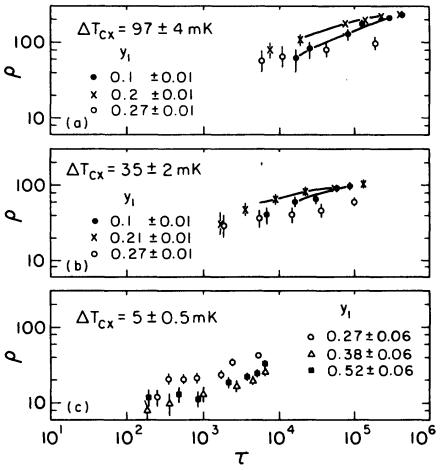

FIG. 9. Experimental values of the scaled mean radius ρ as a function of time for three sample compositions and various initial quench depths as indicated.

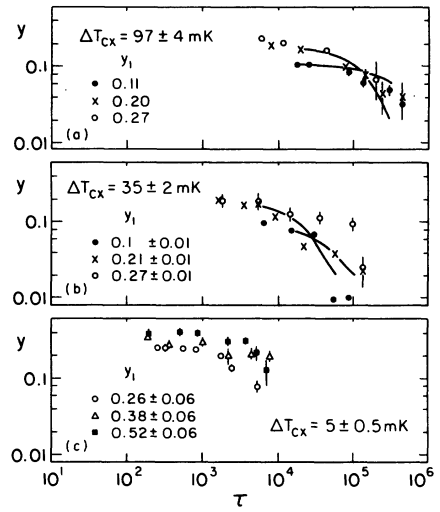

FIG. 10. Experimental values of the relative supersaturation y as a function of time τ for the three sample compositions and various quench depths as indicated.

the results of a simplified growth calculation to be described here. Rather than invoking nucleation theory to calculate the droplet size distribution [from $j(R)$ in the LS theory], its initially observed value is inserted into the diffusion equation for droplet growth, i.e., Eq. (2.5). The equation was integrated numerically with additional constraint of conservation of matter, given by Eq. (2.4). The initial point was so chosen that nucleation could be neglected. This yielded the mean radius R and supersaturation y as a function of time. Coalescence was again neglected and hence our calculations are valid over a limited interval. The calculations were carried out only for phase-separation experiments in which the initial quench depth was small ($y_1 = 0.1$ and 0.2), to assure that coalescence effects were not appreciable, except at very long times. The results appear as solid lines in Figs. 9(a) and 9(b) (ρ vs τ) and in Figs. 10(a) and 10(b) (y vs τ). The agreement with experiment is satisfactory.

V. SUMMARY

Nucleation experiments were conducted in off-critical binary liquid mixtures of 2,6-lutidine and water, a system with an inverted coexistence curve. An optical microscope was used to measure droplet size in the thin portion of a re-entrant cell. The time evolution of the droplet size distribution and number density were determined from microphotographs. The data also yielded the time evolution of the supersaturation. We find that the following hold.

(1) The dynamics of phase separation in the nucleation region depends strongly on the depth of quench δT but not on the initial temperature T_i.

(2) The measurements could not be directly compared with the Langer-Schwartz predictions due to the experimental uncontrollability of the initial quench depth. However, the diffusive growth model for the experimental initial conditions gave results which agreed satisfactorily with experiment, at least for small initial supersaturations, viz., $y_1 = 0.1$ and 0.2.

(3) Coalescence effects due to gravity pose a serious limitation in the study of the dynamics of phase separation in liquid mixtures, at least in the later stages, and especially for deeper quenches. In these experiments we have probed the region which lies between the classical cloud point temperature and the spinodal curve. In this photographic study it was essential to make measurements near the critical point in order to take advantage of the large critical radii and the small nucleation and growth rates.

Our observations of the very initial stages of nucleation were severely limited by our microscopic technique, the finite quench rates, and temperature stability. As a result, our initial goal of verifying the nucleation rate equation [Eq. (2.8)] was not realized. In our view, this same failing characterizes all previous experiments which purported to reveal anomalous supercooling.[3-7] Nevertheless, we believe that the method itself is potentially capable of testing nucleation theory near the critical point.

ACKNOWLEDGMENTS

We have benefited from discussion and correspondence with K. Binder, J. W. Cahn, Y. C. Chou, D. Jasnow, A. Kumar, J. S. Langer, and A. J. Schwartz. One of us (S.K.) would like to thank the Andrew W. Mellon Foundation for support in the form of a fellowship. This work was supported by the National Science Foundation.

[1]J. W. Cahn, Trans. Metall. Soc. AIME 242, 166 (1968).
[2]*Nucleation*, edited by A. C. Zettlemoyer (Marcel Dekker, New York, 1969); J. Frenkel, *Kinetic Theory of Liquids* (Dover, New York, 1946).
[3]B. E. Sundquist and R. A. Oriani, J. Chem. Phys. 36, 2604 (1962).
[4]R. B. Heady and J. W. Cahn, J. Chem. Phys. 58, 896 (1973).
[5]J. S. Huang, W. I. Goldburg, and M. R. Moldover, Phys. Rev. Lett. 34, 639 (1975).
[6]David Dahl and M. R. Moldover, Phys. Rev. Lett. 27, 1421 (1971).
[7]A. J. Schwartz, S. Krishnamurthy, and W. I. Goldburg, Phys. Rev. A 21, 1331 (1980).
[8]Rebekah G. Howland, Ning-Chih-Wong, and Charles M. Knobler, J. Chem. Phys. 73, 522 (1980).
[9]J. S. Langer and L. A. Turski, Phys. Rev. A 8, 3230 (1973).
[10]K. Binder and D. Stauffer, Adv. Phys. 25, 343 (1976).
[11]J. S. Langer and A. J. Schwartz, Phys. Rev. A 21, 948 (1980).
[12]I. Lifshitz and V. Slyozov, J. Phys. Chem. Solids, 19, 35 (1961).
[13]Hewlett Packard Model 2830A sensor oscillator and model 2850 temperature sensor.
[14]Manufactured by Dolan-Jenner Industries, Inc.
[15]Wild, Model M5.
[16]Nikon AFM M-35S with automatic exposure control.
[17]The multiple distilled water and the 2, 6-lutidine were both supplied by Fisher Chemical Company. The latter component was manufactured by Eastman Organic Chemicals, Rochester, N. Y. (Reagent No. 13103).
[18]A. Stein, S. J. Davidson, J. C. Allegra, and G. F. Allen, J. Chem. Phys. 56, 6164 (1972).
[19]E. Gulari, A. F. Colings, R. L. Schmidt, and C. J. Pings, J. Chem. Phys. 56, 6169 (1972).
[20]Walter I. Goldburg, Ching-Hao Shaw, John S. Huang, and Michael S. Pilant, J. Chem. Phys. 68, 484 (1978).

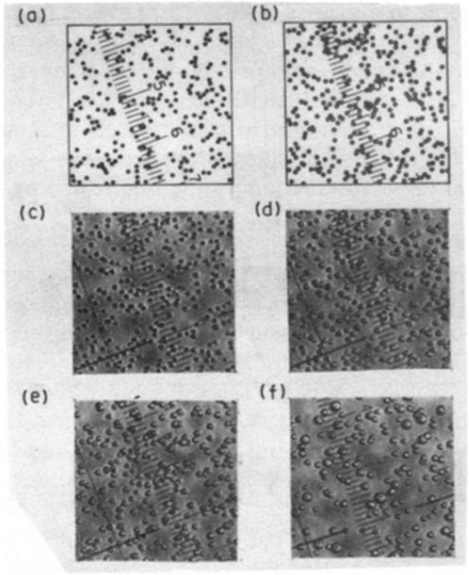

FIG. 2. Microphotographs of nucleating sample at a magnification of 50. The smallest division on the scale is 20 μm. For this run, $\Delta T = 44$ mK and $\delta T = 8$ mK. (a) and (b) are inked reproductions of the original pictures taken 58 and 127 sec after the quench. (c), (d), (e), (f), respectively, are photographs at 5.5, 13.4, 33, and 78 min after the quench.